

Copper Sulfide-Based Plasmonic Photothermal Membrane for High-Efficiency Solar Vapor Generation

Fujun Tao,^{†,‡} Yuliang Zhang,^{*,†,§} Kuan Yin,[†] Shengjia Cao,[†] Xuetong Chang,[†] Yanhua Lei,[†] Dongsheng Wang,[†] Runhua Fan,[†] Lihua Dong,[†] Yansheng Yin,[†] and Xiaobo Chen^{*,†,‡,§}

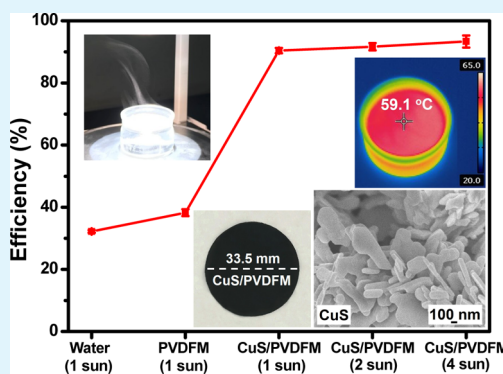
[†]College of Ocean Science and Engineering, Shanghai Maritime University, Shanghai 201306, PR China

[‡]Department of Chemistry, University of Missouri-Kansas City, Kansas City, Missouri 64110, United States

ABSTRACT: Solar vapor generation has attracted tremendous attention as one of the most efficient ways of utilizing solar energy. It is highly desirable to develop low-cost, eco-friendly, and high-efficiency solar absorbers for practical applications of solar vapor generation. Herein, a three-dimensional plasmonic covellite CuS hierarchical nanostructure has been synthesized as the light-absorbing material via a facile one-pot hydrothermal method for structurally integrated solar absorbers with microporous poly(vinylidene fluoride) membrane (PVDFM) as the supporting material. A broadband and highly efficient light absorption has been achieved in the wavelength of 300–2500 nm, along with high water evaporation efficiencies of 90.4 ± 1.1 and $93.3 \pm 2.0\%$ under 1 and 4 sun irradiation, respectively. Meanwhile, stable performance has been demonstrated for over 20 consecutive runs without much performance degradation. To the best of our knowledge, this is the highest performance among the copper sulfide-based solar absorbers.

With the additional features of low-cost and convenient fabrication, this plasmonic solar absorber exhibits a tremendous potential for practical solar vapor generation.

KEYWORDS: *hierarchical CuS, LSPRs, integrated structure, photothermal conversion, solar vapor generation*



1. INTRODUCTION

Over the last few decades, the ever-growing global energy crisis and environmental pollution problems driven by the strong economic growth and ever-increasing pursuit of high quality of life have become serious challenges that human beings are facing today, and renewable energy sources have been attracting considerable attention.^{1–3} Among the known renewable energy sources (e.g., solar energy, wind energy, hydro-energy, and tidal energy), solar energy is the most popular and promising renewable energy because of its abundance and pollution-free nature and has been utilized for a variety of practical applications, such as photocatalysis,^{4–7} solar cells,⁸ and solar-driven energy conversion fields.^{9–15} Among them, solar vapor generation is one of the most straightforward and important pathways to utilize solar energy.^{9,10} Recently, because of the ever-dwindling freshwater resources and the ever-growing demand for fresh water, solar vapor generation has attracted tremendous attention as one of the most important strategies to produce fresh water.¹¹ In conventional solar-driven water evaporation systems, solar energy is usually absorbed by the solar absorbers and converted to thermal energy to heat up a bulk of aqueous water to generate vapor. Obviously, high temperatures occur at the surface of traditional solar absorbers, leading to heat loss by convection or/and solar irradiation and demonstrating a low water evaporation efficiency.^{12,13} For instance, Neumann et al.¹⁴ reported Au nanofluid for solar vapor generation with a

quite low water evaporation efficiency of $\sim 24\%$ under 1.4 sun. As one of the most important indicators for solar vapor generation, the water evaporation efficiency of solar absorber is mainly restricted to its solar light absorption, thermal management, and water transportation.¹⁵ Therefore, it is highly needed to enhance the water evaporation efficiency of the solar absorber. So far, considerable efforts have been made from these three aspects to improve the solar vapor generation efficiency.

Recently, interfacial water evaporation has attracted a lot of attention in improving the water evaporation efficiency.^{16–25} Typically, in such a solar vapor generation system, a solar absorber with free-floating capability self-floats at the water–air interface. This can localize not only the harvesting of solar energy but also the solar vapor generation process at the water–air interface; therefore, the thermal energy is insulated from the bulk aqueous water. The rational structure design of the free-floating solar absorber is usually demonstrated to be membrane systems,^{19–22} paper systems,²³ gauze systems,²⁴ foam systems,^{25,26} wood systems,^{27,28} gels,²⁹ and so forth. Essentially, the capability of harvesting solar energy of the photothermal conversion material of the interfacial solar absorber is the most critical factor for determining the water

Received: July 13, 2018

Accepted: September 18, 2018

Published: October 2, 2018

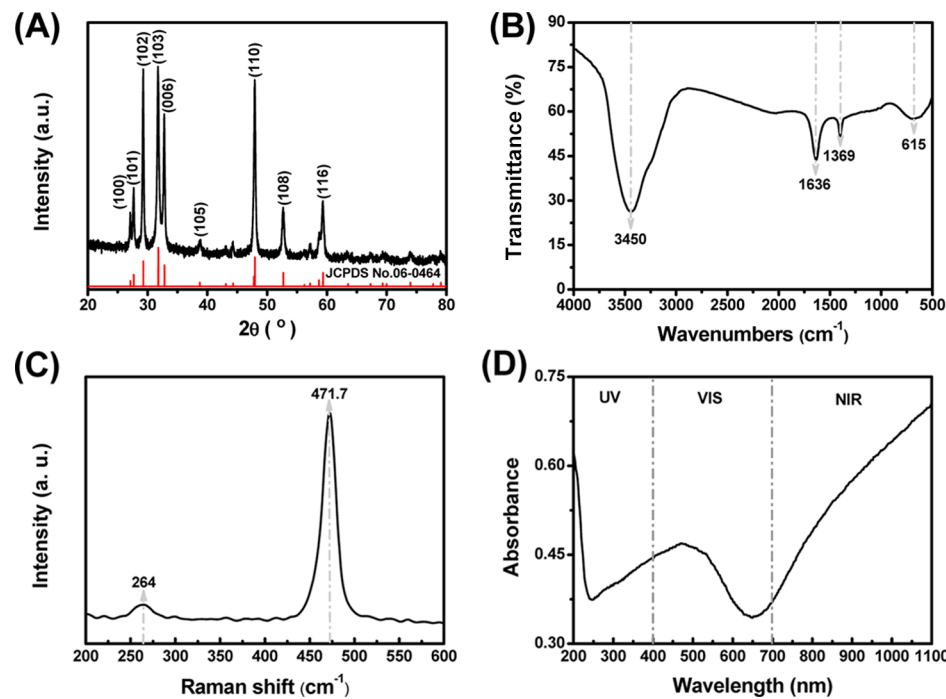


Figure 1. (A) XRD pattern, (B) FTIR spectrum, (C) Raman spectrum, and (D) UV–vis–NIR absorption spectrum of the as-synthesized CuS.

evaporation efficiency.³⁰ Common photothermal conversion materials include plasmonic noble metals (e.g., Au,^{23,31–33} Ag,³⁴ Al³⁵), semiconductor materials,^{19,21,36–39} ceramic-based materials,^{40,41} polymer-based materials,^{29,42} and carbon-based materials.^{43–46} For instance, Fratalocchi et al.³² reported a fully recyclable super-dark metasurface composed of gold nanoparticles, filter paper, and artificial sponge for solar vapor generation with water evaporation efficiencies of ~76 and ~90% under 1 and 3 sun irradiation, respectively. He et al.³³ reported an Au/poly(*p*-phenylene benzobisoxazole) nanofiber composite for solar vapor generation with a water evaporation efficiency of ~83% under 1 sun irradiation. Though appreciable water evaporation efficiencies of the noble-metal based interfacial evaporators have been reported, the noble metals are easily fused together under high temperature because of the long-time solar irradiation, which may cause the degradation of the water evaporation efficiency over time. Moreover, the prices of noble metals are high, which could limit their large-scale production. Higher water evaporation efficiencies have been reported, for example, Liu et al.²⁶ reported a hierarchical graphene foam for solar vapor generation with an efficiency value of ~90% under 1 sun. However, the expensive price of graphene light-harvesting materials could hinder their practical application to some extent. Furthermore, from the view of energy conservation and sustainability for solar-driven applications, the solar light absorption region of the light-harvesting material from visible to infrared (IR) has become ever increasingly important.³⁰ Therefore, in the recent years, active efforts in the development of photothermal conversion material of solar absorber aim to develop materials that possess the capability of broadband solar spectrum absorption to strengthen the utilization efficiency of solar energy and the low-cost and environmental-friendly features for practical application.

Cu_{2-x}S semiconductor materials as one of typical photothermal conversion materials have a wide wavelength range solar absorption in the UV–visible region due to the band gap

absorption, especially with an increased light absorption in the near-IR (NIR) region because of the localized surface plasmon resonances (LSPRs).^{21,36–39} Besides, the Cu_{2-x}S also has the features of low-cytotoxicity, eco-friendly, and outstanding light-stability, which have attracted tremendous attention for the practical application of solar vapor generation.^{21,37,47–49} For instance, Wang et al.⁴⁷ reported a porous integrated structural CuS/polyethylene hybrid membrane for solar vapor generation with a water evaporation efficiency of ~63.5% under 1 sun irradiation. In our previous work,²¹ a CuS/semipermeable collodion membrane (SCM) composite was prepared for solar vapor generation with a water evaporation efficiency of ~68.6% under 1 sun. In addition, Wang et al.⁴⁹ reported Cu_xS /mixed cellulose ester (MCE) films with double-layer structures for solar steam generation with an impressive water evaporation efficiency of ~80% under 1 sun irradiation. Though that was a high water evaporation efficiency of solar irradiation, an obvious major demerit of this double-layer structure is that the Cu_xS located at the top layer via a vacuum filtration method have a tendency to fall off from the MCE membranes under a long-time-lasting irradiation or/and high frequency of usage due to the low adhesion between the photothermal conversion materials of top layer and the supporting materials of bottom layer. In view of these, there is an urgent task for preparing a new solar absorber that not only possesses high water evaporation efficiency but also long-life service to meet the practical requirements for solar vapor generation.

In our work, a novel integrated structural solar absorber composed of plasmonic hierarchical CuS and poly(vinylidene fluoride) membrane (PVDFM) for solar vapor generation is reported. Typically, plasmonic hierarchical CuS prepared via a simple hydrothermal route works as the light-harvesting material and the PVDFM works as the supporting material. As previous reports,^{19,41,42,50,51} PVDFM could be used as an ideal supporting material for the preparation of an interfacial solar absorber because of its numerous advantages, for example, the microporous structure, good hydrophilicity, low

thermal conductivity, low-density, and low-cost. Here, three main limits for water evaporation efficiency could be well improved in our CuS/PVDFM system, for example, broadband and highly efficient solar light absorption (>90%), good thermal management (i.e., low heat loss resulting from the low thermal conductivity of PVDFM), and excellent water transportation system (i.e., good-hydrophilicity for water absorption and the microporous channels for water transport). With these crucial advantages, the CuS/PVDFM could effectively enhance the solar vapor generation efficiency for solar vapor generation. Impressively, the as-prepared CuS/PVDFM enables the water evaporation efficiencies up to $90.4 \pm 1.1\%$ under 1 sun and $93.3 \pm 2.0\%$ under 4 sun, demonstrating the highest efficiency value among the copper sulfide-based solar absorbers as far as we know. Also, it is reused over 20 times without performance degradation. Therefore, the CuS/PVDFM shows a great potential for highly effective solar vapor generation.

2. RESULTS AND DISCUSSION

Figure 1A shows the X-ray diffraction (XRD) pattern of the as-synthesized CuS. The diffraction peaks at 2θ values of 27.1, 27.7, 29.3, 31.8, 32.9, 38.8, 47.9, 52.7, and 59.3 were indexed to the (100), (101), (102), (103), (006), (105), (110), (108), and (116) planes of the hexagonal covellite CuS crystal phase, respectively, matching well with the standard card of JCPDS no. 06-0464 with a space group of $P63/mmc$, cell parameters $a = b = 3.792 \text{ \AA}$ and $c = 16.344 \text{ \AA}$. The sharp and strong intensity diffraction peaks of the as-synthesized CuS indicated a high crystallinity. The absence of any other impurities peaks indicated the high purity of the as-obtained CuS. The bonding information of the as-prepared CuS was probed by Fourier-transform IR (FTIR) spectroscopy, as shown in Figure 1B. Distinct bands were observed near 3450, 1636, 1396, and 615 cm^{-1} . The strong and broad peaks near 3450 and 1636 cm^{-1} were from the stretching and bending modes of O–H and H–O–H groups of the absorbed water molecules.⁵² The peak near 1396 cm^{-1} was assigned to the deformation mode of the O–H bond.²² The peak near 615 cm^{-1} was the characteristic stretching mode of the Cu–S bond of copper sulfide.^{52,53} Raman spectroscopy was used to examine the surface species and spatial variations in composition. Figure 1C shows the obtained Raman spectrum. The peak near 471.7 cm^{-1} was attributed to the covalent S–S bond vibration of S_2 ions at the 4e sites. The strong and sharp Raman peak revealed that the atoms of lattice were aligned in a periodic array. Besides, the broad peak near 264 cm^{-1} was ascribed to the vibration of Cu–S bond. These results were consistent with many previous works.^{54–56} The ultraviolet–visible–NIR (UV–vis–NIR) absorption spectrum of the as-synthesized CuS is presented in Figure 1D in the wavelength range of 200–1100 nm. As is shown, a broad optical absorption in the UV–vis region from 200 to 700 nm and an absorption edge near 650 nm are attributed to the bandgap (~2.0 eV) absorption, and a strong increased light absorption over the NIR region >700 nm is due to the LSPRs of free carrier in CuS nanoparticles.

As shown in the scanning electron microscopy (SEM) images of Figure 2A,B, a hierarchical nanostructure consisting of nanoplates with an average thickness of ~85 nm was observed clearly. Figure 2C shows the typical transmission electron microscopy (TEM) image of CuS. The hierarchical nanostructure is in agreement with the SEM findings. Figure 2D displays the high-resolution TEM (HRTEM) image, which

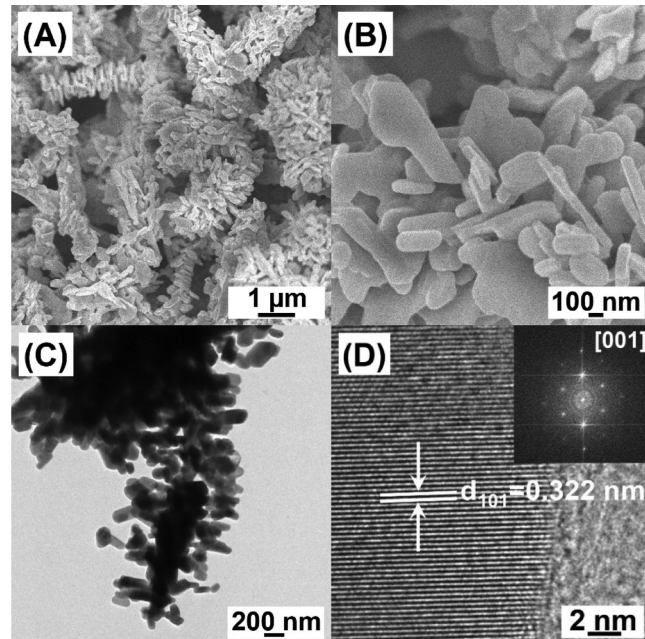


Figure 2. (A) Low-magnification SEM image, (B) high-magnification SEM image, (C) TEM image, (D) HRTEM image, and corresponding FFT pattern (inset) of the as-synthesized CuS nanoparticles, respectively.

showed a lattice fringe distance of ca. 0.322 nm that matched well with the d-spacing of (101) crystal plane of CuS. The corresponding fast Fourier transform (FFT) pattern (inset of Figure 2D) had a highly ordered array of a hexagonal spot, verifying the formation of hexagonal CuS. The strong and bright diffraction dots indicated a highly single crystallinity and were indexed to the [001] direction as the zone axis.

As is well known, the water evaporation efficiency of solar absorber highly depends on its capability of absorbing solar energy. Consequently, the light-absorption capability of the as-prepared CuS/PVDFM was verified from its absorption spectrum, as calculated from its transmission/reflection spectra. As shown in Figure 3A, the white and opaque pure PVDFM (inset of Figure 3A) with a diameter of 33.5 mm demonstrated considerably high diffuse reflection (>95%), near zero transmission, and negligible light absorption (<5%) in the entire solar spectrum, consistent with previous works.^{19,41,42} After gradually loading the hierarchical CuS into PVDFM, the light absorption of CuS/PVDFMs increased with the increased amounts of hierarchical CuS loaded from 1 to 12 mg. However, excess CuS loaded do not increase sharply the light absorption, for example, the light-absorption of 16 mg-CuS/PVDFM is nearly the same as the 12 mg-CuS/PVDFM, as shown in the absorption spectra of Figure 3B. The black 12 mg-CuS/PVDFM (inset of Figure 3B) showed high light absorption in the UV–vis (>90%) and IR region (>96%), indicating that most of the solar energy has been absorbed by the CuS/PVDFM. Interestingly, an increasing slight blue shift (from ca. 600 to 550 nm) of absorption dip is found in the absorption spectra of CuS/PVDFMs with the increasing amounts of hierarchical CuS loaded from 1 to 16 mg, and we speculate that this might be attributed to the increasing light absorption in NIR region due to the LSPRs of plasmonic CuS loaded.

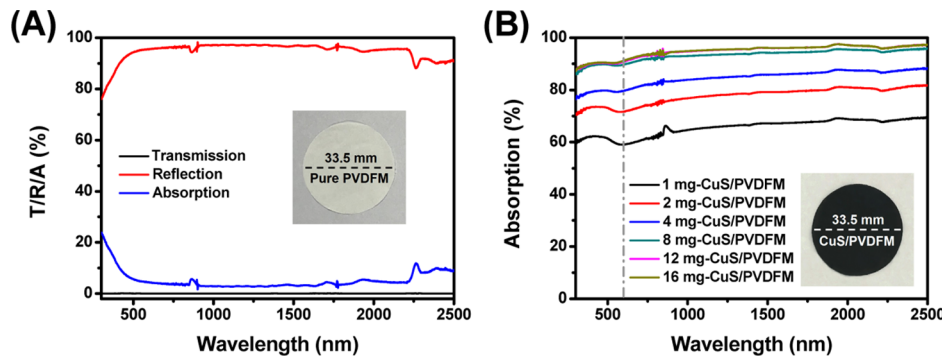


Figure 3. (A) UV–vis–NIR transmission/reflection/absorption spectra and digital photograph (inset) of pure PVDFM, respectively; (B) UV–vis–NIR absorption spectra of the as-prepared CuS/PVDFMs with different contents of CuS, and the digital photograph (inset) of 12 mg-CuS/PVDFM, respectively.

In order to investigate the structure and morphology of the as-prepared 12 mg-CuS/PVDFM, its SEM and optical microscopy images were taken on a field-emission scanning electron microscope (FESEM) and an optical microscope, respectively. As shown in Figure 4A, the open microscale

hydrophilic side is smooth and the hydrophobic side is rough, which is consistent with the previous report.¹⁹

CuS/PVDFMs with various amounts of hierarchical CuS loaded (i.e., 1, 2, 4, 8, 12, and 16 mg per disk) were fabricated as solar absorbers for solar vapor generation. Figure 5A shows the mass change curves within 30 min of pure water under dark environment, 1 sun irradiation, and covered by CuS/PVDFMs with various amounts of hierarchical CuS loaded (i.e., 1, 2, 4, 8, 12, and 16 mg per disk) under 1 sun, respectively. There are two vital indicators (i.e., the efficiency of water evaporation and the rate of water evaporation) to assess the capability of converting the absorbed solar energy to heat energy to generate vapor. According to the previous reports,^{12,21,44,57} the water evaporation efficiencies (η) were calculated by the following eq 1

$$\eta = \frac{\dot{m}h_{fg}}{qA} \quad (1)$$

where \dot{m} denotes the mass flux, h_{fg} represents the enthalpy of the liquid water to vapor phase transition, q is the optical concentration of simulated sunlight irradiation, and A is the mouth area of 40 mm \times 25 mm weighing bottle or the area of the as-prepared CuS/PVDFMs. The dark histograms in Figure 5B exhibited the evaporation efficiencies of the CuS/PVDFMs with different contents of CuS, which followed this order: 1 mg-CuS/PVDFM < 2 mg-CuS/PVDFM < 4 mg-CuS/PVDFM < 8 mg-CuS/PVDFM < 16 mg-CuS/PVDFM < 12 mg-CuS/PVDFM, with the evaporation efficiencies of 56.2, 68.2, 79.0, 85.4, 87.8, and 90.4%, respectively. In comparison, the water evaporation efficiencies were only \sim 32.2 and \sim 38.3% for pure water and pure water covered with pure PVDFM under 1 sun, respectively.

The corresponding water evaporation rates (v) were calculated by eq 2^{20,21,37}

$$v = \frac{m_{\text{loss}}}{\pi \left(\frac{D}{2}\right)^2 t} \quad (2)$$

where m_{loss} denotes the weight of water evaporated, D represents the inner diameter (34.5 mm) of the weighing bottle with a 40 mm \times 25 mm standard or the disk diameter (33.5 mm) of pure PVDFM and the CuS/PVDFMs, and t stands for the solar irradiation time of each solar vapor generation experiment. The gray histograms in Figure 5B showed the water evaporation rates. The water evaporation rates with the increased CuS contents: 0.89, 1.08, 1.25, 1.36,

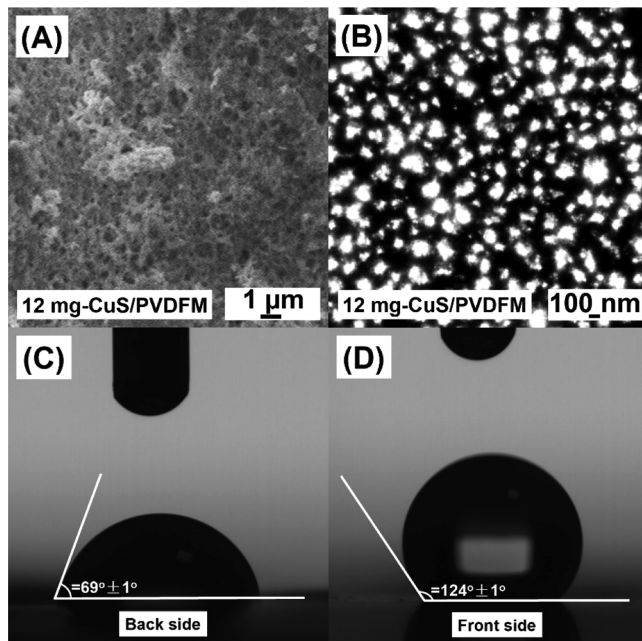


Figure 4. (A) SEM image and (B) optical image of 12 mg-CuS/PVDFM; the surface water contact angles of back (C) and front (D) sides of the 12 mg-CuS/PVDFM, respectively.

porous channels were observed with an average pore size of 150 nm, which were clearly viewed by an optical image as shown in Figure 4B. The hydrophilicity was different for its both sides from the surface contact angle tests. As shown in Figure 4C, the initial surface contact angle was $69 \pm 1^\circ$ for its back side, showing a good water wettability, and was $124 \pm 1^\circ$ (see Figure 4D) for its front side, exhibiting a high hydrophobicity. In the water evaporation process, the back side (hydrophilic side) of the 12 mg-CuS/PVDFM contacting water directly can facilitate the water from the bulk water to the water–air interface and contribute to water transportation. The front side (hydrophobic side) of the 12 mg-CuS/PVDFM contacting air is favorable for localizing heat. Also, this feature is easily differentiated with naked-eye observation that the

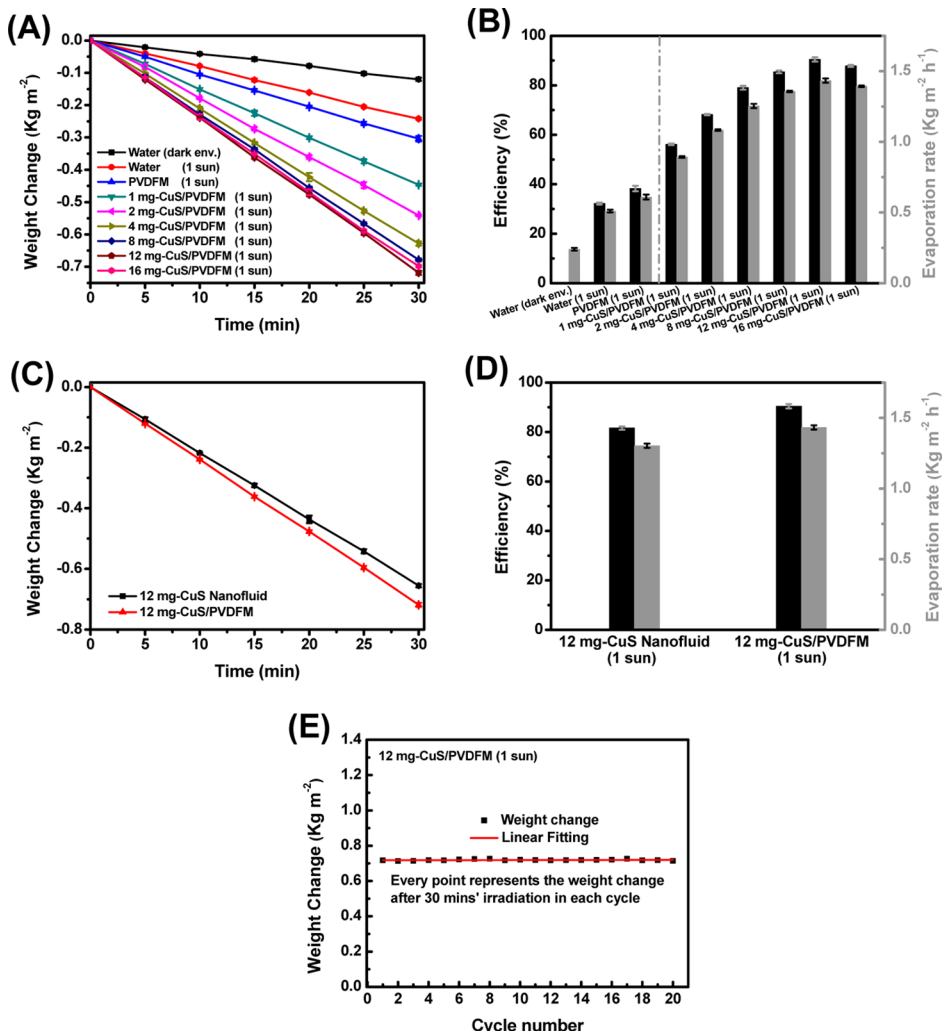


Figure 5. (A) Curves of mass losses using different samples, that is, pure water under dark environment, pure water under 1 sun, pure PVDFM under 1 sun, and CuS/PVDFMs with different contents of hierarchical CuS under 1 sun, respectively; (B) histogram statistics of water evaporation efficiencies (black histograms, the left-hand side axis) of these samples with the corresponding water evaporation rates (gray histograms, right-hand side axis), respectively; (C) mass loss curves of 12 mg-CuS/PVDFM and 12 mg-CuS nanofluid under 1 sun irradiation, respectively; (D) water evaporation efficiencies (black histograms, the left-hand side axis) and water evaporation rates (gray histograms, the right-hand side axis) of 12 mg-CuS/PVDFM and 12 mg-CuS nanofluid, respectively; the data are showed as the average values with error bars. (E) Solar vapor generation cycle performance of 12 mg-CuS/PVDFM under 1 sun irradiation.

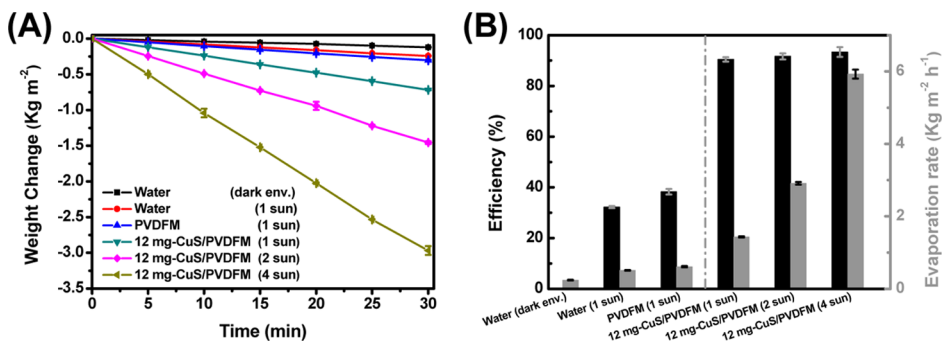


Figure 6. (A) Curves of mass losses of pure water covered by 12 mg-CuS/PVDFM under increasing solar intensities irradiation, that is, 1, 2, and 4 sun, respectively; (B) their corresponding water evaporation efficiencies (black histogram, left-hand side axis) and water evaporation rates (gray histogram, right-hand side axis). For clear comparison, the water evaporation data of pure water under dark environment, pure water under 1 sun, and pure PVDFM under 1 sun were also added, respectively.

1.43, and 1.39 $\text{kg m}^{-2} \text{ h}^{-1}$ for 1, 2, 4, 8, 12, and 16 mg-CuS/PVDFM, respectively. For comparison, the evaporation rates were much less for pure water under dark environment, under

the solar irradiation of 1 sun, and covered by pure PVDFM under the 1 sun. Obviously, as the content of hierarchical CuS increased, the solar vapor generation performance became

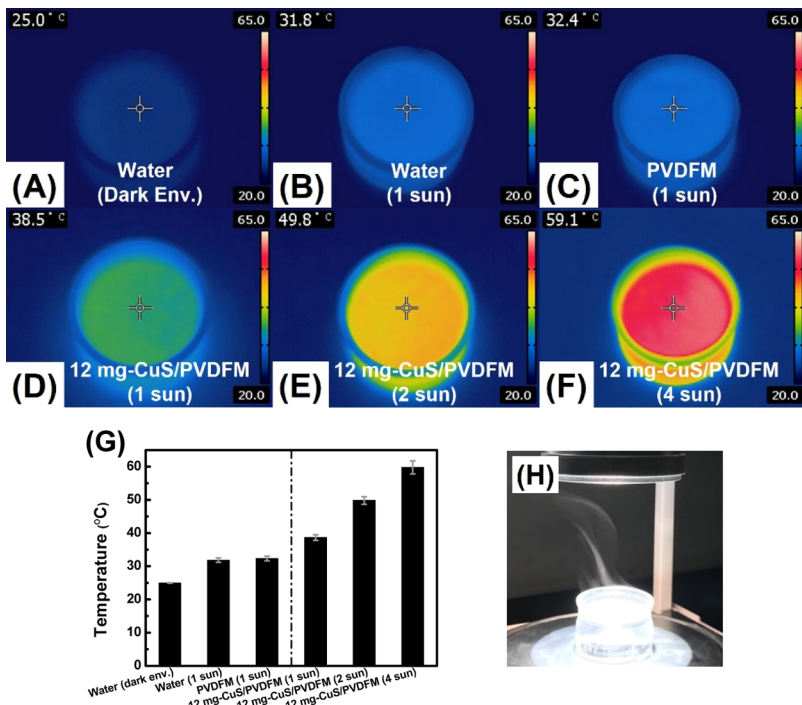


Figure 7. IR images of pure water under dark environment (A) and under 1 sun irradiation (B), respectively; (C) IR image of pure water covered by pure PVDFM under 1 sun irradiation; (D–F) IR images of pure water covered by 12 mg-CuS/PVDFM under different solar intensities irradiation. (G) Corresponding histogram statistics of their surface temperature. (H) Picture of water vapor generated under 4 sun irradiation.

Table 1. Comparison of Solar Vapor Generation Performance of Various Solar Absorbers

solar absorbers	classification of photothermal conversion materials	power density (kW m^{-2})	efficiencies (%)	temperature of vapor generation ($^{\circ}\text{C}$)	refs
modified graphene/aerogel	carbon-based	1	76.9 ± 2.5	~80	11
exfoliated graphite/carbon foam	carbon-based	1	~64	~50	12
CNT/GO/nanofibrillated cellulose	carbon-based	1	85.6	~36.5	16
GO/MCE membrane/PS foam	carbon-based	1	~80	~38.8	18
RGO/MCE membrane	carbon-based	1	~60	~38.8	22
reduced graphene oxide/PS foam	carbon-based	1	~83	~83	25
hierarchical graphene foam	carbon-based	1	~91.4	~55	26
carbonized wood	carbon-based	1	~72	~43	28
3D graphene foam	carbon-based	1	~87	~40	43
carbon nanotube/cellulose nanofibrils	carbon-based	1	76.3	~32.7	44
carbonized mushrooms	carbon-based	1	~78	~38	46
graphite powder/SCM	carbon-based	1.5	~56.8	~39.9	20
PPy/HNG	polymer-based	1	~94	~41.3	29
PPy/PVDFM	Polymer-based	1	~93.8	~88	42
Au/nanoporous alumina template	plasmonic metal-based	1	~49	~38	31
Au/filter paper/artificial sponge	plasmonic metal-based	1	~76	~35	32
Au/PBO nanofiber	plasmonic metal-based	1	83	~32	33
Au/airlaid-paper	plasmonic metal-based	4.5	~77.8	~80	23
Al nanoparticles/AAO	plasmonic metal-based	1	~57.5	~42	35
TiN/ceramic fiber wool	plasmonic ceramic-based	1	>80	~42	40
Ti ₃ C ₂ /PVDFM	plasmonic ceramic-based	1	84	~75	41
black Al–Ti–O/PVDFM	plasmonic semiconductor-based	1	~77.52	~47.5	19
CuS/PVDFM	plasmonic semiconductor-based	1	90.4 ± 1.1	~38.5	this work

better from 1 to 12 mg, followed by an inflection point appeared, the low solar vapor generation performance of the CuS/PVDFM with 16 mg hierarchical CuS loaded versus 12 mg-CuS/PVDFM was probably owing to the blockage of water transport channel routes (i.e., the microscale porous channels)

of PVDFM by the hierarchical CuS. In summary, the 12 mg-CuS/PVDFM showed the best solar vapor generation performance under 1 sun.

The solar vapor generation performance of CuS/PVDFM was also compared to that of the CuS nanofluid. Figure 5C

Table 2. Comparison of Solar Vapor Generation Performance of the Solar Absorbers Based on Plasmonic Semiconductor-Copper Sulfides

solar absorbers	light sources	power density (kW m^{-2})	efficiencies (%)	temperatures of vapor generation ($^{\circ}\text{C}$)	refs
CdS-Cu ₇ S ₄ composite film	solar simulator	1.5	~48.4		37
CuS/polyethylene hybrid membrane	solar simulator	1	~63.9	~37.6	47
CuS/SCM	solar simulator	1	~68.6	~35.2	21
Cu ₇ S ₄ nanocrystal film	infrared lamp	1	~77.1		48
CuS/MCE membrane	solar simulator	1	80 \pm 2.5	~42.8	49
CuS/PVDFM	solar simulator	1	90.4 \pm 1.1	~38.5	this work

shows the mass loss curves of 12 mg-CuS/PVDFM and 12 mg-CuS nanofluid; clearly, CuS/PVDFM had a larger water evaporated weight than the CuS nanofluid. Meanwhile, CuS/PVDFM had a higher water evaporation efficiency (90.4 vs 81.7%) than the CuS nanofluid as shown in Figure 5D, and a higher water evaporation rate (1.43 vs $1.3 \text{ kg m}^{-2} \text{ h}^{-1}$). Therefore, the CuS/PVDFM shows a better performance than the CuS nanofluid for solar vapor generation, besides the obvious benefit of good reusability over the nanofluid, which has a big difficulty of gathering the photothermal conversion material after a solar vapor generation experiment.

The durability and reusability of solar absorber is an important indicator for the practical application of solar vapor generation. To test its reusability, the solar vapor generation experiments of 12 mg-CuS/PVDFM were measured over 20 cycles under the same conditions. As shown in Figure 5E, all water evaporated weights were close to 0.717 kg m^{-2} , indicating an excellent durability.

The solar vapor generation performance was also examined under a series of light intensities irradiation, that is, 1, 2, and 4 sun. As shown in Figure 6A, the mass losses increased dramatically with increased light intensities from 1 to 4 sun, so did the water evaporation efficiencies and water evaporation rates as shown in Figure 6B. Specifically, the water evaporation efficiencies were 90.4, 91.7, and 93.3% with the corresponding water evaporation rates of 1.43, 2.91, and $5.93 \text{ kg m}^{-2} \text{ h}^{-1}$ under 1, 2, and 4 sun irradiation, respectively. The average water evaporation rate of $5.93 \text{ kg m}^{-2} \text{ h}^{-1}$ was 4.15, 9.72, 11.63, and 24.71 times higher than that of pure water covered by CuS/PVDFM under 1 sun irradiation, of pure water covered by pure PVDFM under 1 sun irradiation, of pure water under the irradiation of 1 sun, and of pure water under dark environment, respectively.

In addition, IR photography was used to record the surface temperature variation of pure water covered by the CuS/PVDFM during the solar vapor generation process. During each solar vapor generation experiment, the initial temperature of pure water was near 25°C , that is, the ambient temperature. After each water evaporation experiment, the photograph was captured using an IR camera. Figure 7A–C shows the photographs of the surface temperature of pure water under dark environment, under 1 sun irradiation, and covered by pure PVDFM under the irradiation of 1 sun, respectively. Correspondingly, the surface temperatures were about 25.0, 31.8, and 32.4°C , respectively. As shown in Figure 7D–F, the surface temperature sharply increased with increased solar intensity from 1 to 4 sun. Specifically, the surface temperatures were about 38.5, 49.8, and 59.1°C under the irradiation of 1, 2, and 4 sun, respectively. Therefore, we speculate that the surface temperature would be further higher under a solar simulator irradiation with higher output power. For clear comparison, the histogram statistics of the surface temperature

are shown in Figure 7G. Figure 7H shows the picture for the water vapor generation under the stimulated sunlight of 4 sun. Clearly, the water vapor generated was observed.

For comparison, Tables 1 and 2 summarized part of the solar vapor generation efficiencies and the temperatures of vapor generation under solar simulator of the recent reports. Obviously, the water evaporation efficiency of CuS/PVDFM reported in this work is ~90.4% under 1 sun, which ranked highly in these related research works. However, there is no direct correlation between the interfacial temperatures and their solar vapor generation efficiencies. Though the temperature of vapor generation is not the direct factor for the water evaporation efficiency, it is an important indicator to assess the photothermal conversion performance of the interfacial evaporators and to evaluate the potential for different practical applications, for example, sterilization of waste and desalination of seawater. In addition, compared with the currently reports^{21,37,47–49} based on copper sulfides for water evaporation (see Table 2), the water evaporation efficiency of our new solar absorber is, to the best of our knowledge, the highest ranking.

3. CONCLUSIONS

A novel solar absorber comprising hierarchical CuS and PVDFM has been demonstrated as an ideal candidate for highly effective solar vapor generation. This solar absorber is prepared by systematic design strategies that satisfy the requirements for interfacial solar vapor generation, including plasmonic hierarchical CuS for heat concentration, low-density PVDFM for free floatation at the air–water interface, the hydrophilic side of CuS/PVDFM for water absorption, the microporous structure of CuS/PVDFM for water transport, the hydrophobic side of CuS/PVDFM for localizing heat, the low thermal conductivity for decreasing the heat loss, and an excellent reusability for long-life service. The CuS/PVDFM demonstrates high water evaporation efficiencies of $90.4 \pm 1.1\%$ under 1 sun and $93.3 \pm 2.0\%$ under 4 sun irradiation, respectively. Besides, the cyclic tests verify that the CuS/PVDFM can be recycled over 20 times, demonstrating an excellent durability and reusability. The CuS/PVDFM is low-cost, easy to prepare, and reusable, therefore offering a new designing strategy for solar vapor generation, and shows great potential for many other practical applications, such as desalination of seawater, treatment of sewage, and other solar-heating technologies.

4. EXPERIMENTAL SECTION

4.1. Materials. All chemicals and solvents were of analytical reagent grade and used as starting materials without any further purification. Copper chloride dihydrate ($\text{CuCl}_2 \cdot 2\text{H}_2\text{O}$), thiourea (Tu), *N,N*-dimethylformamide (DMF), and ethanol ($\text{C}_2\text{H}_5\text{O}$) were purchased from Sinopharm Chemical Reagent Co. Ltd. (Shanghai,

China). PVDF was provided from Xiya Reagent Co. Ltd (Shandong, China). Deionized water was obtained from a Milli-Q system (Millipore).

4.2. Synthesis of Hierarchical CuS. The hierarchical CuS was synthesized via a facile one-pot hydrothermal reaction, using $\text{CuCl}_2 \cdot 2\text{H}_2\text{O}$ and thiourea (Tu) as starting materials. In a typical reaction, 0.12 mmol (0.02 g) $\text{CuCl}_2 \cdot 2\text{H}_2\text{O}$ was dissolved sufficiently in a 50 mL beaker containing 10 mL aqueous solution under sonication treatment. Then, 10 mL of aqueous solution containing 0.26 mmol (0.02 g) thiourea was added into the above solution, and the mixture was sonicated in an ultrasonic bath for 3–5 min to form a homogenous solution. Subsequently, the 20 mL mixture solution was transferred into a Teflon-lined stainless-steel autoclave with a 25 mL capacity. The mixture solution was sealed in an autoclave and treated at 180 °C for 18 h in an oven. After the reaction, the stainless-steel autoclave was cooled to room temperature naturally. The resulting black precipitate was collected by centrifugation and washed with deionized water and ethanol several times, respectively. Next, the collected black precipitate was dried in a vacuum oven at 50 °C for several hours until the sample was dried thoroughly.

4.3. Membrane Preparation. Disk-shaped PVDFMs containing different contents of hierarchical CuS were fabricated via the reported method with a slight modification.^{19,46,47} First, preparation of PVDF/DMF solution: 1 g of PVDF powder was added slowly into 15 mL of DMF solution and stirred constantly for 1 h at room temperature. Next, 174 mg of CuS powder was added into a 10 mL beaker containing 1 mL of PVDF/DMF solution, which was sonicated using an ultrasonic bath for 5 min and stirred at ambient condition for 30 min to form homogenous mixture solution. The above-obtained CuS/PVDF/DMF mixture solution was dislodged by using a 1000 μL pipette and transferred to the surface of a flat glass, which was cast by a scraper with a gap of 150 μm and then immersed in a bath containing deionized water for 1 h. As a result, the membrane could be removed easily from the flat glass. In order to remove the residual traces of solvent or additives, the membrane was taken out from the bath and washed with ethanol several times. Finally, the membrane was dried in a vacuum oven at 50 °C for 2 h. The as-prepared CuS/PVDFM was trimmed into a disk in accordance with a disk-shaped mold with a diameter of 33.5 mm. Therefore, the CuS/PVDFM with the amount of 12 mg CuS loaded (i.e., 12 mg-CuS/PVDFM) was prepared, respectively. The fabrication method was also used for fabricating other control samples, for example, 1 mg-CuS/PVDFM, 2 mg-CuS/PVDFM, 4 mg-CuS/PVDFM, 8 mg-CuS/PVDFM, 16 mg-CuS/PVDFM, and pure PVDFM (i.e., without any hierarchical CuS loaded).

4.4. Characterization. The powder XRD pattern was obtained on an X'Pert Pro diffractometer (PaNalytical, Holland) with Cu K α irradiation ($\lambda = 1.5418 \text{ \AA}$) at 40 kV voltage and 40 mA current, which was recorded over the angular range from 20° to 80°. The SEM images were obtained on an FESEM system (JSM-6700F). The TEM, HRTEM, and FFT characterizations were carried out on a JEOL JEM-2100F TEM system. The Fourier transform IR spectrum was collected using a FTIR spectrometer (Vertex 70, Bruker). The Raman measurement was performed via a SENTERRA II Compact Raman Microscope (Bruker, Germany) with a laser excitation wavelength of 532 nm at 5 mW. The UV-vis-NIR absorbance spectrum was recorded on a UV-vis-NIR scanning spectrophotometer (Lambda 35, PerkinElmer). The UV-vis-NIR transmittance and diffuse reflectance spectra were recorded with a UV-vis-NIR scanning spectrophotometer equipped with an integrating sphere (Lambda 950, PerkinElmer). The optical microscopy image was taken by a Leica microscope (DMS00, Germany). The contact angles were measured using a JC2000D1 contact-angle analyzer (Shanghai Zhongchen Digital Technic Apparatus Co. Ltd, China). The surface temperature distribution and IR thermal images were captured using a E40 FLIR camera (FLIR Systems, Inc., America).

4.5. Solar Vapor Generation. During the solar vapor generation process, a container (40 mm × 25 mm weighing bottle with an inner diameter of 34.5 mm) containing 20 mL of deionized water was prepared. The hydrophilic side (called back side) of the disk-shaped

CuS/PVDF membrane ($D = 33.5 \text{ mm}$) was placed face down to make it contact water inside the container directly, and correspondingly, the hydrophobic side (called front side) was placed upward to contact air. The solar beam was provided from a chamber optical measurement system composed of a PLS-SXE300/300UV solar simulator with tunable light-density output (Perfect Light Technology Co. Ltd, Beijing, China) and other optical components. The light intensities of 1–4 sun ($\text{kW}\cdot\text{m}^{-2}$) were calibrated using a VLP-2000 optical power meter (Ranbond Technology Co., Ltd, Beijing, China). The weight changes from water evaporation were recorded using a 4-decimal electronic precision balance (FR224CN, OHRUS) for 30 min at intervals of 5 min. Besides, other solar vapor generation experiments, for example, 12 mg-CuS nanofluid comprising 12 mg of CuS and 20 mL of deionized water under 1 sun irradiation and pure water covered by 12 mg-CuS/PVDFM under an increased output light-densities irradiation (i.e., from 1 sun, to 2 sun, and 4 sun irradiation) were measured, respectively. For comparison, the solar vapor generation experiments of pure water covered by pure PVDFM under 1 sun irradiation, pure water under 1 sun irradiation, and pure water under dark environment were also tested, respectively. Moreover, in order to certify the durability and reusability of the CuS/PVDFM, the water evaporation process of 12 mg-CuS/PVDFM was measured for 20 cycles under the same experimental conditions. For each cycle, the experiment process of 12 mg-CuS/PVDFM was irradiated under a light irradiation of 1 sun for 30 min along with an interval time of 30 min for the next cycle. The wetted 12 mg-CuS/PVDFM was dried in a vacuum oven at 50 °C.

AUTHOR INFORMATION

Corresponding Authors

*E-mail: yizhang@shmtu.edu.cn (Y.Z.).

*E-mail: chenxiaoobo@umkc.edu (X.C.).

ORCID

Yuliang Zhang: [0000-0001-7205-7768](https://orcid.org/0000-0001-7205-7768)

Xiaobo Chen: [0000-0002-7127-4813](https://orcid.org/0000-0002-7127-4813)

Notes

The authors declare no competing financial interest.

ACKNOWLEDGMENTS

X.C. appreciates the support from the U.S. National Science Foundation (DMR-1609061) and the College of Arts and Sciences, University of Missouri—Kansas City. Y.Z. and X.C. acknowledge the National Key R & D Program of China (nos. 2016YFB0300700 and 2016YFB0300704); Y.Y. acknowledges the State Key Development Program for Basic Research of China (973 program, no. 2014CB643306); X.C. acknowledges the NSF of Shanghai (no. 17ZR1440900); Y.L. acknowledges the National Nature Science Foundation of China (no. S1602195); and F.T. acknowledges the Doctoral Innovation Foundation of SMU (no. 2016ycx037) and the Doctoral Excellent Thesis Project Foundation of SMU (no. 2017BXLP005).

REFERENCES

- (1) Schloegl, R. Fuel for thought. *Nat. Mater.* **2008**, *7*, 772–774.
- (2) Chu, S.; Majumdar, A. Opportunities and Challenges for a Sustainable Energy Future. *Nature* **2012**, *488*, 294–303.
- (3) Lewis, N. S.; Nocera, D. G. Powering the Planet: Chemical Challenges in Solar Energy Utilization. *Proc. Natl. Acad. Sci. U.S.A.* **2006**, *103*, 15729–15735.
- (4) Chen, X.; Liu, L.; Yu, P. Y.; Mao, S. S. Increasing Solar Absorption for Photocatalysis with Black Hydrogenated Titanium Dioxide Nanocrystals. *Science* **2011**, *331*, 746–750.
- (5) Wang, Z.; Yang, C.; Lin, T.; Yin, H.; Chen, P.; Wan, D.; Xu, F.; Huang, F.; Lin, J.; Xie, X.; Jiang, M. Visible-Light Photocatalytic, Solar

- Thermal and Photoelectrochemical Properties of Aluminium-Reduced Black Titania. *Energy Environ. Sci.* **2013**, *6*, 3007–3014.
- (6) Wang, Z.; Yang, C.; Lin, T.; Yin, H.; Chen, P.; Wan, D.; Xu, F.; Huang, F.; Lin, J.; Xie, X.; Jiang, M. H-doped Black Titania with Very High Solar Absorption and Excellent Photocatalysis Enhanced by Localized Surface Plasmon Resonance. *Adv. Funct. Mater.* **2013**, *23*, 5444–5450.
- (7) Lin, T.; Yang, C.; Wang, Z.; Yin, H.; Lü, X.; Huang, F.; Lin, J.; Xie, X.; Jiang, M. Effective Nonmetal Incorporation in Black Titania with Enhanced Solar Energy Utilization. *Energy Environ. Sci.* **2014**, *7*, 967–972.
- (8) Liao, Y.; Liu, H.; Zhou, W.; Yang, D.; Shang, Y.; Shi, Z.; Li, B.; Jiang, X.; Zhang, L.; Quan, L. N.; Quintero-Bermudez, R.; Sutherland, B. R.; Mi, Q.; Sargent, E. H.; Ning, Z. Highly Oriented Low-Dimensional Tin Halide Perovskites with Enhanced Stability and Photovoltaic Performance. *J. Am. Chem. Soc.* **2017**, *139*, 6693–6699.
- (9) Tian, Y.; Zhao, C. Y. A Review of Solar Collectors and Thermal Energy Storage in Solar Thermal Applications. *Appl. Energy* **2013**, *104*, 538–553.
- (10) Zeng, J.; Xuan, Y. Enhanced Solar Thermal Conversion and Thermal Conduction of MWCNT-SiO₂/Ag Binary Nanofluids. *Appl. Energy* **2018**, *212*, 809–819.
- (11) Fu, Y.; Wang, G.; Ming, X.; Liu, X.; Hou, B.; Mei, T.; Li, J.; Wang, J.; Wang, X. Oxygen Plasma Treated Graphene Aerogel as a Solar Absorber for Rapid and Efficient Solar Steam Generation. *Carbon* **2018**, *130*, 250–256.
- (12) Ghasemi, H.; Ni, G.; Marconnet, A. M.; Loomis, J.; Yerci, S.; Miljkovic, N.; Chen, G. Solar Steam Generation by Heat Localization. *Nat. Commun.* **2014**, *5*, 4449.
- (13) Shang, W.; Deng, T. Solar Steam Generation: Steam by Thermal Concentration. *Nat. Energy* **2016**, *1*, 16133.
- (14) Neumann, O.; Urban, A. S.; Day, J.; Lal, S.; Nordlander, P.; Halas, N. J. Solar Vapor Generation Enabled by Nanoparticles. *ACS Nano* **2013**, *7*, 42–49.
- (15) Dao, V.-D.; Choi, H.-S. Carbon-Based Sunlight Absorbers in Solar-Driven Steam Generation Devices. *Global Chall.* **2018**, *2*, 1700094.
- (16) Li, Y.; Gao, T.; Yang, Z.; Chen, C.; Luo, W.; Song, J.; Hitz, E.; Jia, C.; Zhou, Y.; Liu, B.; Yang, B.; Hu, L. 3D-Printed, All-in-One Evaporator for High-Efficiency Solar Steam Generation under 1 Sun Illumination. *Adv. Mater.* **2017**, *29*, 1700981.
- (17) Liu, G.; Xu, J.; Wang, K. Solar Water Evaporation by Black Photothermal Sheets. *Nano Energy* **2017**, *41*, 269–284.
- (18) Li, X.; Xu, W.; Tang, M.; Zhou, L.; Zhu, B.; Zhu, S.; Zhu, J. Graphene Oxide-Based Efficient and Scalable Solar Desalination under One Sun with a Confined 2D Water Path. *Proc. Natl. Acad. Sci. U.S.A.* **2016**, *113*, 13953–13958.
- (19) Yi, L.; Ci, S.; Luo, S.; Shao, P.; Hou, Y.; Wen, Z. Scalable and Low-cost Synthesis of Black Amorphous Al-Ti-O Nanostructure for High-Efficient Photothermal Desalination. *Nano Energy* **2017**, *41*, 600–608.
- (20) Tao, F.; Zhang, Y.; Wang, B.; Zhang, F.; Chang, X.; Fan, R.; Dong, L.; Yin, Y. Graphite Powder/Semipermeable Collodion Membrane Composite for Water Evaporation. *Sol. Energy Mater. Sol. Cells* **2018**, *180*, 34–45.
- (21) Tao, F.; Zhang, Y.; Cao, S.; Yin, K.; Chang, X.; Lei, Y.; Fan, R.; Dong, L.; Yin, Y.; Chen, X. CuS Nanoflowers/Semipermeable Collodion Membrane Composite for High-Efficiency Solar Vapor Generation. *Mater. Today Energy* **2018**, *9*, 285–294.
- (22) Wang, G.; Fu, Y.; Ma, X.; Pi, W.; Liu, D.; Wang, X. Reusable Reduced Graphene Oxide Based Double-Layer System Modified by Polyethylenimine for Solar Steam Generation. *Carbon* **2017**, *114*, 117–124.
- (23) Liu, Y.; Yu, S.; Feng, R.; Bernard, A.; Liu, Y.; Zhang, Y.; Duan, H.; Shang, W.; Tao, P.; Song, C.; Deng, T.; Reusable. A Bioinspired, Reusable, Paper-Based System for High-Performance Large-Scale Evaporation. *Adv. Mater.* **2015**, *27*, 2768–2774.
- (24) Liu, Y.; Chen, J.; Guo, D.; Cao, M.; Jiang, L. Floatable, Self-Cleaning, and Carbon-Black-Based Superhydrophobic Gauze for the Solar Evaporation Enhancement at the Air-Water Interface. *ACS Appl. Mater. Interfaces* **2015**, *7*, 13645–13652.
- (25) Shi, L.; Wang, Y.; Zhang, L.; Wang, P. Rational Design of a Bi-Layered Reduced Graphene Oxide Film on Polystyrene Foam for Solar-Driven Interfacial Water Evaporation. *J. Mater. Chem. A* **2017**, *5*, 16212–16219.
- (26) Ren, H.; Tang, M.; Guan, B.; Wang, K.; Yang, J.; Wang, F.; Wang, M.; Shan, J.; Chen, Z.; Wei, D.; Peng, H.; Liu, Z. Hierarchical Graphene Foam for Efficient Omnidirectional Solar-Thermal Energy Conversion. *Adv. Mater.* **2017**, *29*, 1702590.
- (27) Jiang, F.; Li, T.; Li, Y.; Zhang, Y.; Gong, A.; Dai, J.; Hitz, E.; Luo, W.; Hu, L. Wood-Based Nanotechnologies Toward Sustainability. *Adv. Mater.* **2018**, *30*, 1703453.
- (28) Xue, G.; Liu, K.; Chen, Q.; Yang, P.; Li, J.; Ding, T.; Duan, J.; Qi, B.; Zhou, J. Robust and Low-Cost Flame-Treated Wood for High-Performance Solar Steam Generation. *ACS Appl. Mater. Interfaces* **2017**, *9*, 15052–15057.
- (29) Zhao, F.; Zhou, X.; Shi, Y.; Qian, X.; Alexander, M.; Zhao, X.; Mendez, S.; Yang, R.; Qu, L.; Yu, G. Highly Efficient Solar Vapour Generation via Hierarchically Nanostructured Gels. *Nat. Nanotechnol.* **2018**, *13*, 489–495.
- (30) Zhu, L.; Gao, M.; Peh, C. K. N.; Ho, G. W. Solar-Driven Photothermal Nanostructured Materials Designs and Prerequisites for Evaporation and Catalysis Applications. *Mater. Horiz.* **2018**, *5*, 323–343.
- (31) Zhou, L.; Zhuang, S.; He, C.; Tan, Y.; Wang, Z.; Zhu, J. Self-Assembled Spectrum Selective Plasmonic Absorbers with Tunable Bandwidth for Solar Energy Conversion. *Nano Energy* **2017**, *32*, 195–200.
- (32) Liu, C.; Huang, J.; Hsiung, C.-E.; Tian, Y.; Wang, J.; Han, Y.; Fratalocchi, A. High-Performance Large-Scale Solar Steam Generation with Nanolayers of Reusable Biomimetic Nanoparticles. *Adv. Sustainable Syst.* **2017**, *1*, 1600013.
- (33) Chen, M.; Wu, Y.; Song, W.; Mo, Y.; Lin, X.; He, Q.; Guo, B. Plasmonic Nanoparticle-Embedded Poly(*p*-phenylene benzobisoxazole) Nanofibrous Composite Films for Solar Steam Generation. *Nanoscale* **2018**, *10*, 6186–6193.
- (34) Wang, H.; Miao, L.; Tanemura, S. Morphology Control of Ag Polyhedron Nanoparticles for Cost-Effective and Fast Solar Steam Generation. *Sol. RRL* **2017**, *1*, 1600023.
- (35) Zhou, L.; Tan, Y.; Wang, J.; Xu, W.; Yuan, Y.; Cai, W.; Zhu, S.; Zhu, J. 3D Self-Assembly of Aluminium Nanoparticles for Plasmon-Enhanced Solar Desalination. *Nat. Photonics* **2016**, *10*, 393–398.
- (36) Liang, G.; Jin, X.; Qin, H.; Xing, D. Glutathione-Capped, Renal-Clearable CuS Nanodots for Photoacoustic Imaging and Photothermal Therapy. *J. Mater. Chem. B* **2017**, *5*, 6366–6375.
- (37) Tao, F.; Zhang, Y.; Zhang, F.; Wang, K.; Chang, X.; An, Y.; Dong, L.; Yin, Y. From CdS to Cu₃S₄ Nanorods via a Cation Exchange Route and Their Applications: Environmental Pollution Removal, Photothermal Conversion and Light-Induced Water Evaporation. *ChemistrySelect* **2017**, *2*, 3039–3048.
- (38) Tao, F.; Zhang, Y.; Zhang, F.; An, Y.; Dong, L.; Yin, Y. Structural Evolution from CuS Nanoflowers to Cu₉S₅ Nanosheets and Their Applications in Environmental Pollution Removal and Photothermal Conversion. *RSC Adv.* **2016**, *6*, 63820–63826.
- (39) Tao, F.; Zhang, Y.; Zhang, F.; Yang, L.; An, Y.; Yin, Y. Influence of Potassium Chloride on the Structure of Cu₉S₅ Nanosheets with Hexagonal Holes. *Mater. Lett.* **2015**, *140*, 166–169.
- (40) Kaur, M.; Ishii, S.; Shinde, S. L.; Nagao, T. All-Ceramic Microfibrous Solar Steam Generator: TiN Plasmonic Nanoparticle-Loaded Transparent Microfibers. *ACS Sustainable Chem. Eng.* **2017**, *5*, 8523–8528.
- (41) Li, R.; Zhang, L.; Shi, L.; Wang, P. MXene Ti₃C₂: An Effective 2D Light-to-Heat Conversion Material. *ACS Nano* **2017**, *11*, 3752–3759.
- (42) Wang, Y.; Wang, C.; Song, X.; Huang, M.; Megarajan, S. K.; Shaukat, S. F.; Jiang, H. Improved Light-Harvesting and Thermal Management for Efficient Solar-Driven Water Evaporation Using 3D Photothermal Cones. *J. Mater. Chem. A* **2018**, *6*, 9874–9881.

- (43) Yang, Y.; Zhao, R.; Zhang, T.; Zhao, K.; Xiao, P.; Ma, Y.; Ajayan, P. M.; Shi, G.; Chen, Y. Graphene-Based Standalone Solar Energy Converter for Water Desalination and Purification. *ACS Nano* **2018**, *12*, 829–835.
- (44) Jiang, F.; Liu, H.; Li, Y.; Kuang, Y.; Xu, X.; Chen, C.; Huang, H.; Jia, C.; Zhao, X.; Hitz, E.; Zhou, Y.; Yang, R.; Cui, L.; Hu, L. Lightweight, Mesoporous, and Highly Absorptive All-Nanofiber Aerogel for Efficient Solar Steam Generation. *ACS Appl. Mater. Interfaces* **2018**, *10*, 1104–1112.
- (45) Ding, H.; Peng, G.; Mo, S.; Ma, D.; Sharshir, S. W.; Yang, N. Ultra-Fast Vapor Generation by a Graphene Nano-Ratchet: A Theoretical and Simulation Study. *Nanoscale* **2017**, *9*, 19066–19072.
- (46) Xu, N.; Hu, X.; Xu, W.; Li, X.; Zhou, L.; Zhu, S.; Zhu, J. Mushrooms as Efficient Solar Steam-Generation Devices. *Adv. Mater.* **2017**, *29*, 1606762.
- (47) Shang, M.; Li, N.; Zhang, S.; Zhao, T.; Zhang, C.; Liu, C.; Li, H.; Wang, Z. Full-Spectrum Solar-to-Heat Conversion Membrane with Interfacial Plasmonic Heating Ability for High-Efficiency Desalination of Seawater. *ACS Appl. Energy Mater.* **2018**, *1*, 56–61.
- (48) Zhang, C.; Yan, C.; Xue, Z.; Yu, W.; Xie, Y.; Wang, T. Shape-Controlled Synthesis of High-Quality Cu₇S₄ Nanocrystals for Efficient Light-Induced Water Evaporation. *Small* **2016**, *12*, 5320–5328.
- (49) Guo, Z.; Ming, X.; Wang, G.; Hou, B.; Liu, X.; Mei, T.; Li, J.; Wang, J.; Wang, X. Super-hydrophilic copper sulfide films as light absorbers for efficient solar steam generation under one sun illumination. *Semicond. Sci. Technol.* **2018**, *33*, 025008.
- (50) Politano, A.; Argurio, P.; Di Profio, G.; Sanna, V.; Cupolillo, A.; Chakraborty, S.; Arafat, H. A.; Curcio, E. Photothermal Membrane Distillation for Seawater Desalination. *Adv. Mater.* **2017**, *29*, 1603504.
- (51) Fontananova, E.; Jansen, J. C.; Cristiano, A.; Curcio, E.; Drioli, E. Effect of Additives in the Casting Solution on the Formation of PVDF Membranes. *Desalination* **2006**, *192*, 190–197.
- (52) Saranya, M.; Santhosh, C.; Ramachandran, R.; Kollu, P.; Saravanan, P.; Vinoba, M.; Jeong, S. K.; Grace, A. N. Hydrothermal Growth of CuS Nanostructures and Its Photocatalytic Properties. *Powder Technol.* **2014**, *252*, 25–32.
- (53) Nie, G.; Zhang, L.; Lu, X.; Bian, X.; Sun, W.; Wang, C. A One-Pot and in Situ Synthesis of CuS-Graphene Nanosheet Composites with Enhanced Peroxidase-Like Catalytic Activity. *Dalton Trans.* **2013**, *42*, 14006–14013.
- (54) Wang, S.; Jiao, S.; Wang, J.; Chen, H.-S.; Tian, D.; Lei, H.; Fang, D.-N. High-Performance Aluminum-Ion Battery with CuS@C Microsphere Composite Cathode. *ACS Nano* **2017**, *11*, 469–477.
- (55) Adhikari, S.; Sarkar, D.; Madras, G. Hierarchical Design of CuS Architectures for Visible Light Photocatalysis of 4-Chlorophenol. *ACS Omega* **2017**, *2*, 4009–4021.
- (56) Hurma, T.; Kose, S. XRD Raman Analysis and Optical Properties of CuS Nanostructured Film. *Optik. Int. J. Light. Electron. Optic.* **2016**, *127*, 6000–6006.
- (57) Ni, G.; Li, G.; Boriskina, S. V.; Li, H.; Yang, W.; Zhang, T.; Chen, G. Steam Generation under One Sun Enabled by a Floating Structure with Thermal Concentration. *Nat. Energy* **2016**, *1*, 16126.